PCCP

Accepted Manuscript

ROYAL SOCIETY OF CHEMISTRY

www.rsc.org/pccp

PCCP

RSCPublishing

ARTICLE

Ketocyanine Dyes: Impact of Conjugation length on Optical Absorption and Third-Order Polarizabilities

Cite this: DOI: 10.1039/xoxxoooooox

Kada Yesudas,[a, b,*] Eluvathingal D. Jemmis[a, c] and Kottamarthi Bhanuprakash[d]

Received ooth March 2015,
Accepted ooth xxxxx 2015

DOI: 10.1039/xoxxoooooox

www.rsc.org/

Broken symmetry and symmetry adapted cluster-configuration interaction techniques help to understand the structure-property relationships like impact of conjugation length on the electronic structure, small energy optical absorption and third-order polarizabilities in symmetric ketocyanine dyes. The sum-over-states approximation truncated to essential states model helped to understand the origin of negative sign and the most relevant components of average static third-order polarizabilities. The results can be used as a design principle to model the ketocyanine dyes which can absorb in the visible to NIR region and show large negative third-order nonlinear activity.

1. Introduction

Linear conjugated organic molecules are the most widely studied among the various classes of functional dyes. Topologically, they belong to one of the two classes, either cyanine–like or polyene–like carbon chains. Cyanines (CY), Scheme 1, contain odd number of carbon atoms in the backbone and the π-system of these compounds is uniformly extended over the whole carbon chain and has zero degree of bond length alternation (BLA). Polyenes, on the other hand, contain an even number of carbon atoms (odd number of conjugated bonds) and show a very pronounced π–electron bond alternation in the ground state.

CY dyes are relatively stable, and have high molar absorption coefficients (~10^{-5} M^{-1} cm^{-1}), medium fluorescence intensity, narrow spectrum width and the ability to form H– or J–aggregates.[1, 2] The maximum absorption wavelength of CY can be tuned precisely from visible to near-infrared (NIR) region by chemical structural modifications. These unique photophysical and photochemical properties make CY dyes useful in many potential applications such as nonlinear optics (NLO),[3-5] optical data storage,[6, 7] probes for biological systems,[8-10] dye lasers,[11, 12] photorefractive materials,[13, 14] and photodynamic therapy.[15-17]

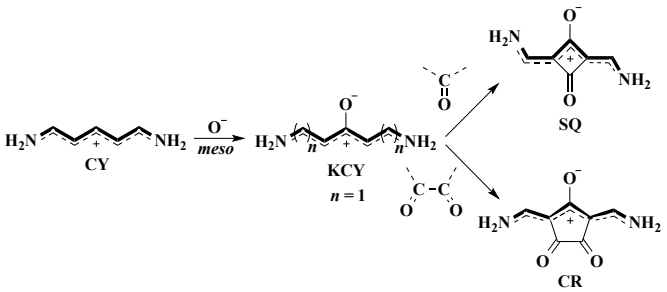

Scheme 1 Systematic perturbation of CY to obtain KCY, SQ and CR dyes.

The substitution of the hydrogen atom at the *meso*-position of CY by O^- gives rise to a ketocyanine (KCY) like chromophore, Scheme 1. This in turn perturbs the distribution of π-electrons and depending on the extent of π-conjugation; the energy gap between the Frontier molecular orbitals (FMOs) is reduced. Substitution of *meso*-1 and *meso*+1 hydrogen atoms with >C=O and -(C=O)-(O=C)- give rise to squaraine (SQ) and croconate (CR) dyes (scheme 1). Synthesis of such KCY dyes is of current research interest due to their interesting molecular properties and serve as key components in various high-tech applications such as absorption in the long wavelength region (800-1100 nm),[18-20] nonlinear optics,[21-25] dye sensitized solar cells,[26-29] energy transfer cascades,[30, 31] fluorescence biolabeling,[32, 33] electronic devices and so on.[34-36]

Among the above mentioned applications of KCY dyes, the electronic absorption in the NIR region and NLO properties have been extensively studied because of their potential applications in electronic and optical devices.[3] Since the chromophoric carbon chain of KCY, SQ and CR contains odd number of methine units, the spectroscopic and photophysical properties are expected to be similar to that of CY. A large number of experimental and theoretical studies have been carried out to understand the structure-property relationships in these molecules.[37] One of the earliest calculations based on MNDO (modified neglect of differential overlap) and CNDO/s (complete neglect of differential overlap/spectroscopic, single + double energy selected configuration interaction) proposed that the small energy absorption (1.98 eV) in SQ is due to the donor-acceptor-donor (D-A-D) type of chromophoric structure.[38] Similarly, using simple Huckel Molecular Orbital (HMO) calculations and orbital symmetry considerations, Momicchioli et al. have pointed out that SQ containing even number of methine units show small HOMO-LUMO gap (HLG) while those with odd number of methine units show a large gap.[39] In addition, our previous studies showed that these molecules are biradicaloids based on the charge transfer analysis of the excited state (excitation from $S_0 \rightarrow S_1$) by using the symmetry-adopted cluster-configuration interaction (SACCI)[40-45] method and from the numerical biradical index (Y_i) as well. Also, they showed a linear correlation between the biradical character and the optical absorption, and third-order polarizabilities.[41, 43]

Theoretically, different models can be used to understand these systems. In view of the complexity of these molecules, the density functional theory (DFT)[46-48] and time dependent (TD) DFT[49, 50] methods would be of first choice. However, it has been shown that standard hybrid and generalized gradient approximation (GGA) type functionals fail in the description of the electronic spectra of CYs and KCYs.[51, 52] Moreover both the absorption and NLO properties depend on the molecular geometries. Recently, it has been shown that density functionals with full exact exchange produce geometries with considerable accuracy and help to find the crossover point for the transition of CY from symmetric to assymetric structure and its impact over the lowest optical absorption and third-order polarizabilities.[53] However, there is no detailed study about the correlation between the general structure-property relationships of KCY and the evolution of lowest optical absorption and third-order polarizabilities, which is the main goal of this work. Here we present different computational models and to predict the structure-property relationships in KCYs to explain the NIR absorption and large third-order polarizabilities.

2. Computational Details

All the calculations in this work have been carried out by using the Gaussian 09 *ab initio*/DFT quantum chemical package.[54] The molecular geometries in the singlet ground state (S_0) are energy minimized with C_2 symmetry constraints using the hybrid DFT-B3LYP functional.[55] The theoretical equilibrium S_0 state geometries are obtained when the maximum internal forces acting on all the atoms and the stress are less than 4.5×10^{-4} eV/Å and 1.01×10^{-3} kBar respectively. The obtained geometries are found to be minima on the potential energy surface (PES) characterized by the real values for vibrational frequencies at the same Hessian. The energy minimization of the triplet state (T_1) geometries were also performed to check the relative stability of the S_0 state. Broken symmetry (BS) approach at Hartree-Fock (HF) level is used to obtain the natural orbital occupancies of the HOMO and LUMO and to calculate the numerical values of the biradical index (Y_i). These calculations were performed with Poples's triple-ξ quality 6-311G basis set with *p* and *d* polarization functions.

SACCI[56-58] studies at level two have been performed to obtain $S_0\rightarrow S_1$ and $S_0\rightarrow S_2$ transition energies (E_{01} and E_{02}); S_0 and S_1 permanent dipole moments (μ_0 and μ_1); and $S_0\rightarrow S_1$ and $S_1\rightarrow S_2$ transition dipole moments, (μ_{01} and μ_{12}). An active CI-space of 160 orbitals (in 1:3 ratio for occupied and unoccupied) were included to obtain the energies of the lowest 10 excited states (five states in each symmetry element). The molecular orbitals presented and used for the discussion are based on the HF level in order to be consistent with the SACCI ordering of the molecular orbitals where HF orbitals are the starting point. Pople's double-ξ quality 6-31G basis set with *p* and *d* polarization functions was employed for these calculations.

Finally the average static third-order polarizabilities, ⟨γ⟩ (nonlinearity at zero-photon energy, representing the off-resonant value) are computed using sum-over states[59] approach of Orr and Ward truncated to a three-state model (essential states model) as shown in eq.(1) to eq.(3).[37] The longitudinal components γ_{xxxx}, γ_{yyyy} and γ_{zzzz} were obtained using eq.(1) and the cross components γ_{xxyy}, γ_{xxzz} and γ_{yyzz} were obtained using the eq.(2). The ⟨γ⟩ is then obtained using eq.(3). In general, the first, second and third terms in the eq. (1) and (2) are designated as the dipolar (D), one-photon or negative (N) and two-photon (T) terms respectively.

$$\gamma_{iiii} = 24\left[\frac{\left(\mu_{01}^{i}\Delta\mu_{01}^{i}\right)^2}{\left(E_{01}\right)^3} - \frac{\left(\mu_{01}^{i}\right)^4}{\left(E_{01}\right)^3} + \frac{\left(\mu_{01}^{i}\right)^2\left(\mu_{12}^{i}\right)^2}{\left(E_{01}\right)^2 E_{02}}\right] = \gamma_{iiii}^{D} + \gamma_{iiii}^{N} + \gamma_{iiii}^{T} \quad \text{eq.(1)}$$

$$\gamma_{iijj} = 4\left[\frac{4\mu_{01}^{i}\mu_{01}^{j}\Delta\mu_{01}^{i}\Delta\mu_{01}^{j} + \left(\mu_{01}^{i}\Delta\mu_{01}^{j}\right)^2 + \left(\mu_{01}^{j}\Delta\mu_{01}^{i}\right)^2}{\left(E_{01}\right)^3} - \frac{6\left(\mu_{01}^{i}\mu_{01}^{j}\right)^2}{\left(E_{01}\right)^3} + \frac{4\mu_{01}^{i}\mu_{12}^{i}\mu_{01}^{j}\mu_{12}^{j} + \left(\mu_{01}^{i}\Delta\mu_{12}^{j}\right)^2 + \left(\mu_{01}^{j}\Delta\mu_{12}^{i}\right)^2}{\left(E_{01}\right)^2 E_{02}}\right] = \gamma_{iijj}^{D} + \gamma_{iijj}^{N} + \gamma_{iijj}^{T} \quad \text{eq.(2)}$$

$$\langle\gamma\rangle = \frac{1}{5}\left(\sum\gamma_{iiii} + 2\sum\gamma_{iijj}\right) \quad \text{eq.(3)}$$

where $i \in (x, y, z)$.

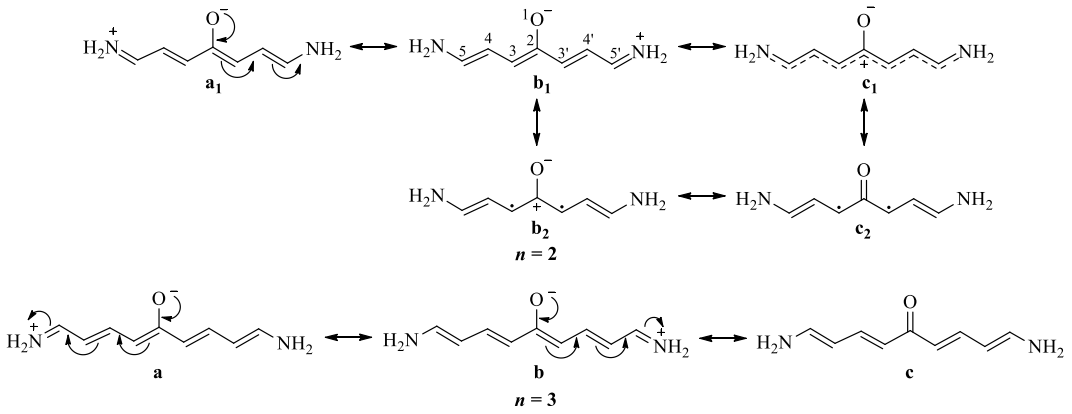

Fig. 1 Resonance structures of odd (n_o) and even (n_e) series of KCYs.

3. Results and Discussion

3.1. Energy and Wavefunction Stability

The geometry optimization of the series of KCYs in their ground state with singlet closed shell (SCS) configuration were performed by increasing a single methine unit at a time symmetrically (Scheme 1, KCY structure). For easy understanding, the KCY series is separated into two sub-series i.e., odd (n_o = 1, 3, 5 and 7) and even (n_e = 2, 4, 6 and 8) series respectively. The odd series contains odd number of methine units on either side of CO while even series contain even number of methine units as shown in Fig. 1. It should be noted that while counting the number of methine units, the core oxyallyl part should be excluded. The resonance structures for the shortest of its kinds i.e., n_e = 2 and n_o = 3 are shown in Fig. 1. The

resonance structures $\mathbf{a_1}$ and $\mathbf{b_1}$ for n_e series represent two valence bond structures, in which the positive charge is localized on one of the nitrogen atoms resulting charge-separated structures, whereas in $\mathbf{c_1}$, the positive charge is delocalized over the entire carbon chain as in a typical CY. The other possibility is that either it exists in a hybrid structure $\mathbf{b_2}$, a hybrid form of biradical and charge-separated structures, or in a neutral biradical structure $\mathbf{c_2}$. The resonance structures **a** and **b** for n_o series are exactly similar to that of n_e series resulting in charge-separated structures, while the structure **c** is characterized by alternating π-bonds (absence of charge-separation) and posses cross-conjugation (the set of π bonds in aminopolyeneal chromophore interact with each other by conjugation excluding the other aminopolyene chomophore from interaction).

In view of the earlier predictions that in general these systems are biradicaloids (non-interacting) in nature,[41, 43] the wavefunction stability of the SCS configuration were therefore performed.[60] The eigen values of stability matrix produced real values with a magnitude of 0.085, 0.056, 0.040 and 0.031 for n_o series and imaginary values with almost equal magnitude of ~-0.027 for n_e series as shown in Table **1**. The detailed meaning of these eigen values can be found in the original paper,[60] but in general, imaginary eigen values indicate instability in the corresponding wavefunction and represents a saddle point on the PES. This signifies that in the ground state of n_e series, a strong static (non-dynamical) correlation effect plays an important role.[61] Describing such systems with single determinant methods like restricted (R)HF or RDFT yield poor description of the ground state wavefunctions and thus require an alternative method. One of the methods is the BS approach, which corrects the static correlation approximately at lower computation cost.[62-64] The unrestricted (U)HF or UDFT allow for spin-symmetry breaking and approximate the static correlation correction by splitting the α and β electrons into two different orbitals.[65, 66] Thus, the geometries of both KCY series were reoptimized at the singlet open shell (SOS) configuration using BS approach at UB3LYP. This resulted in relatively stable wavefunctions which are lower in energy than their corresponding SCS analogue for n_e series. The calculated energy difference $\Delta E_1 = {}^1E_{SOS} - {}^1E_{SCS}$ is shown in Table **1** and the values increased with increasing n_e (-2.58, -4.65, -5.84 and -6.65 kcal/mole for n_e = 2, 4, 6 and 8) while there is no energy lowering (ΔE_1 = 0.0 kcal/mole) or invoked structural changes, in comparison to the CSC configuration of n_o series.

Table 1 Calculated relative energy between the singlet closed and open shell configurations (ΔE_1), spin projected open shell singlet and singlet closed shell (ΔE_2) and spin projected open shell singlet and triplet state (ΔE_3) in kcal/mole, eigen values of the stability matrix and spin contamination values ($\langle S^2 \rangle$).

n	[a]ΔE_1	[b]ΔE_2	[c]ΔE_3	Stability	$\langle S^2 \rangle$
n_o					
1	0.00	0.00	-72.34	0.085	0.00
3	0.00	0.00	-53.60	0.056	0.00
5	0.00	0.00	-43.72	0.040	0.00
7	0.00	0.00	-37.67	0.031	0.00
n_e					
2	-2.58	-4.98	-7.99	-0.022	0.61
4	-4.65	-6.43	-4.60	-0.027	0.81
6	-5.84	-7.21	-3.11	-0.029	0.92
8	-6.65	-7.72	-2.28	-0.029	1.00

[a] $\Delta E_1 = {}^1E_{SOS} - {}^1E_{SCS}$; [b] $\Delta E_2 = {}^1E_{SOS\text{-}AP} - {}^1E_{SCS}$; [c] $\Delta E_3 = {}^1E_{SOS\text{-}AP} - {}^3E_{T1}$

It is also worth noting that the singlet biradical form of n_e series is largely contaminated by higher spin states; $\langle S^2 \rangle$ values are different from 0 (pure singlet) or 2 (pure triplet) as shown in Table **1**. The spin contamination of the biradical state grows from 0.61–1.00 and this may be the likely result of the energy gap between the S_0 and T_1 states becoming smaller as the size of n_e increases. Although $\langle S^2 \rangle$ is not rigorously defined in DFT, spin contamination makes additional stability of the singlet open shell configuration (biradical form) relative to the singlet closed shell configuration. However, a heavily spin contaminated wavefunction[67-69] in principle will affect properties such as total energy, optimized geometry and excited state energies and so on, as it originates in the unrestricted wavefunction itself. In order to eliminate this error, the approximate spin projection (AP) technique has been used where the total energy is given by eq.(4):

$$ {}^{LS}E(AP) = {}^{LS}E(BS) + \frac{{}^{LS}E - {}^{HS}E}{{}^{HS}\langle \hat{S}^2 \rangle - {}^{LS}\langle \hat{S}^2 \rangle} \left({}^{LS}\langle \hat{S}^2 \rangle - {}^{LS}\langle \hat{S}^2 \rangle_{exact} \right) \quad \text{eq.4} $$

The quantities ${}^{LS}E$ and ${}^{HS}E$ in the above equation are the total energies of low and high spin states.[67-69] The energy of the SOS wavefunction within this approximation for n_e series is further lowered energetically by 1.07–2.40 kcal/mole (ΔE_2) and hence increase in the S_0–T_1 energy gap (ΔE_3). No energy lowering or increase of ΔE_3 is observed for n_o series. However, in both the series, the energy gap is decreased with increase in number of methine units. Beyond n_e = 8, the SOS configuration becomes unstable and T_1 becomes relatively more stable than S_0. Similarly, the stability of T_1 for n_o can be seen after 17-methine units in the aminopolymethine chain (linear fit).

3.2. Soliton Structure and Bond Length Alternation:

As shown in Scheme 1, the KCY and its derivatives have same number of methine units in the carbon backbone as in CY. CYs possess a distinguishing feature of alternating charges (charge wave or soliton),[70, 71] thus a similar charge wave is expected in KCYs. Alternately, the soliton can be described as a function of charge alternation at the neighbouring π-centres; $\Delta q = |q_i - q_{i+1}|$, where q is the charge at i^{th} π-center.[71, 72] Fig. **2** shows plots of q_i and Δq_i based on the Mulliken atomic charges and reveals the following facts. (i) The presence of oxygen atom at the *meso*-position of the carbon backbone in KCYs reduced charge at the *meso*-carbon atom by 0.55 e. (ii) Both the odd and even series showed charge alternation. Except at C_4, C_5 and $C_{4'}$, $C_{5'}$ positions in even series, charge alternation is not observed (shaded region in Fig. **2**). (iii) The attenuation of the soliton from the centre is very slow compared to CY with same carbon chain length.[53]

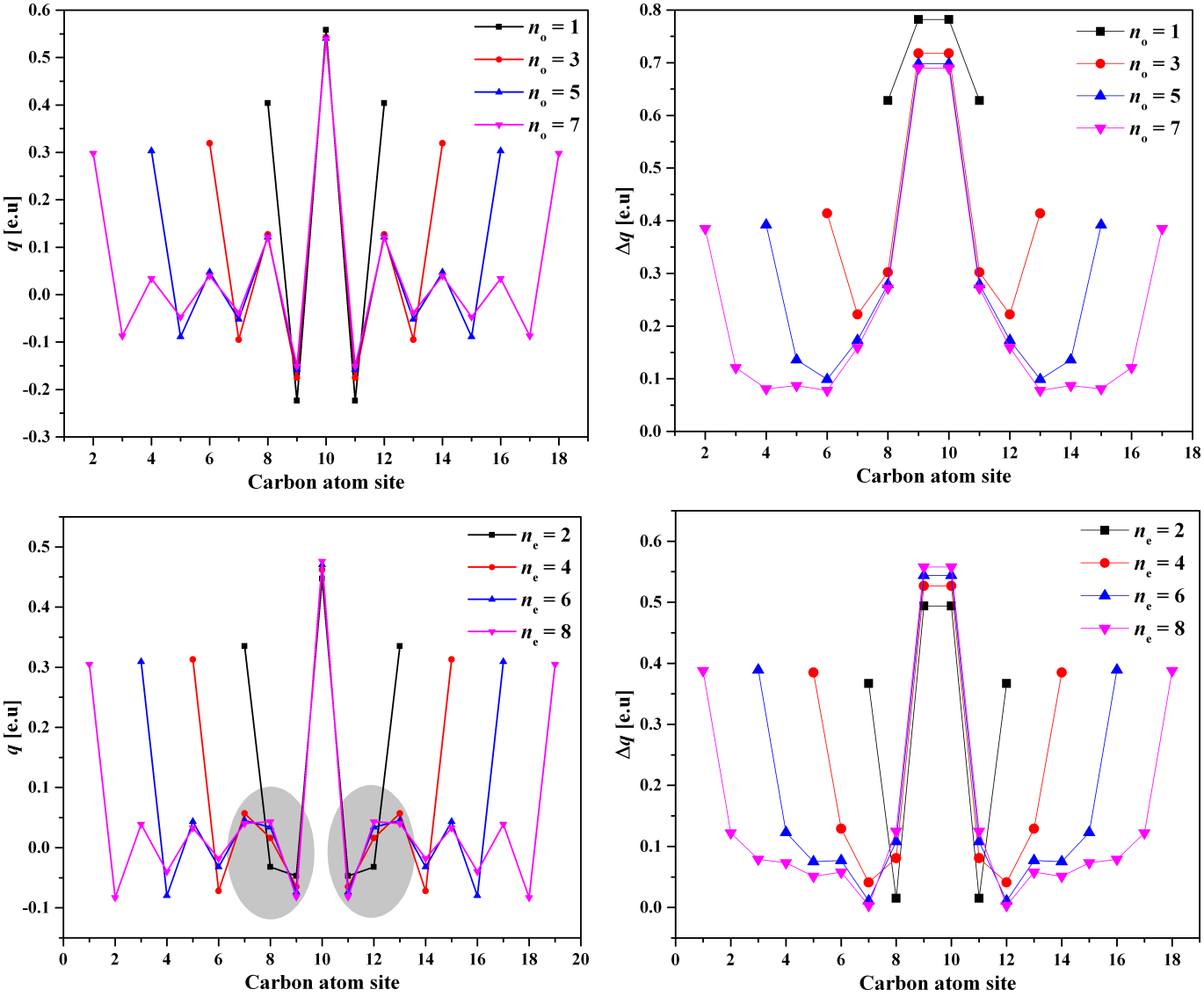

Fig. 2 Charge alternations in the n_o and n_e series of KCYs.

The local bond length alternation of the neighbouring C–C bonds described by $\Delta l = |l_i - l_{i+1}|$, where l is the length of the i^{th} C–C bond in the back bone.[71] The corresponding Δl values for each of the cyanine series is shown in Fig. **3**. The Δl in the case of n_o series for $(C_2–C_3)–(C_3–C_4)$ is almost constant with a value in between 0.122–0.125 Å and for the remaining Δl along the carbon chain for each n_o, a constant value of ~0.078 Å is obtained. This is in line with the resonance structure **c** in Fig. **1**. Further increase in n_o would not give a significant rise in BLA suggesting the saturation limit. Contrary to the n_o series, the n_e series showed a different behaviour as evident from the Δl values. The $(C_2–C_3)–(C_3–C_4)$ bond distance is continuously increased with n_e by 0.056–0.101 Å, while the rest of the Δl in each n_e is continuously increased except at $(C_4–C_5)–(C_5–C_6)$ in n_e = 6 and $(C_5–C_6)–(C_6–C_7)$ in n_e = 8, the increase is very small (BLA of ~0.003 Å).

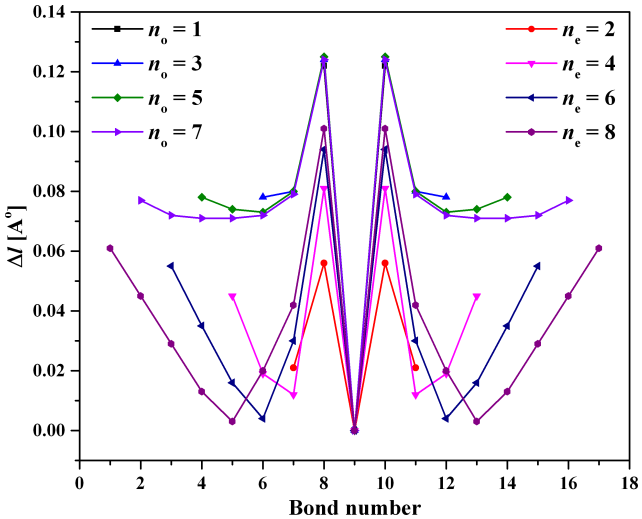

Fig. 3 Local BLA in the n_o and n_e series of KCYs.

3.3. Singlet Biradical Character:

According to the values of ΔE_1 and ΔE_2 in Table **1**, KCYs corresponding to the n_e series are biradicals, the less favorable singlet states which are best described by the SB method and qualitatively show pronounced biradical character. A singlet biradical can be defined as a molecular species that has all electrons paired, but a pair of these electrons occupies different parts of space with a small shared region, Fig. **4**. The ground state of such species is a singlet, yet they exhibit biradical character. On the other hand, a pure biradical is a molecular species with two electrons occupying two degenerate, or nearly degenerate, molecular orbitals.

Quantitatively, the numerical values of the biradical character in the singlet ground state are estimated using the SB approach at UHF level and the obtained values are presented in Table **2**.[73] The biradical index Y_i, related to the HOMO and LUMO for singlet states, is defined by the weight of the doubly-excited configuration in the multi-configuration (MC)-SCF theory, and is formally expressed in the case of the spin-projected UHF (PUHF) theory as[74]

$$Y_i = 1 - \frac{2T_i}{1+T_i^2}$$

where T_i is the orbital overlap between the corresponding orbital pairs, and can be calculated using the occupation numbers of UHF natural orbitals.

$$T_i = \frac{\eta_{\mathrm{HOMO}} - \eta_{\mathrm{LUMO}}}{2}$$

It is worth pointing out that the biradical index ranges from 0 % for the SCS configuration to 100 % for the pure biradical state. As n_o series is stable in SCS configuration, it has Y_i of 0 %. The Y_i value for n_e series is found in the range between ~53–86 %. In addition, Y_i increases with decrease in orbital overlap T_i. It turns out that, in spite of the simplicity of the scheme using the unrestricted natural orbitals (UNOs), it successfully reproduced the biradical character of the investigated molecules. Also, it is seen that Y_i is linearly dependent on the C_3–C_2–$C_{3'}$ bond angle, which is in line with our earlier predictions.[43] For n_o series, a constant value of 115.9° is obtained while for n_e series, it increased by a very small value of ~0.37° and range between 112.2–113.3°, suggesting that a very small increase in angle is sufficient to produce large Y_i in the S_0 state.

Table 2 The C_3–C_2–$C_{3'}$ angle (∠, °), natural orbital occupations of HOMO, LUMO (η_{HOMO}, η_{LUMO}), orbital overlap (T_i), percent biradical character (%Y_i) and HOMO-LUMO gap (HLG, eV) for both the series of KCYs.

n	∠C_3–C_2–$C_{3'}$	η_{HOMO}	η_{LUMO}	T_i	%Y_i	HLG
n_o						
1	115.9	2.000	0.000	1.000	0	4.77
3	115.9	1.827	0.173	0.827	2	3.66
5	115.9	1.652	0.348	0.652	8	3.06
7	115.9	2.000	0.000	1.000	0	2.68
n_e						
2	112.2	1.250	0.750	0.250	53	1.59
4	112.5	1.146	0.854	0.146	71	1.16
6	112.9	1.098	0.902	0.098	81	0.92
8	113.3	1.072	0.928	0.071	86	0.76

The spatial biradical distribution is examined in the singlet biradical structures by inspecting the HOMOs and LUMOs for the α and β spin electrons. The frontier orbitals for the α and β spin electrons of n_o = 5 and n_e = 6, calculated using the SB method are depicted in Fig. **4**. The α-HOMO and β-HOMO, as well as the α-LUMO and β-LUMO, are of almost identical shapes for n_o = 5 (Fig. **4**, top). The HOMO and LUMO are occupied with 1.652 and 0.348 electrons, respectively. In addition, there is a noticeable shared region between the HOMO and LUMO, which is in agreement with the large T_i value of 0.652 (Table **2**). The situation is quite different in n_e = 6 (Fig. **4**, bottom). A remarkable feature is that the α-HOMO and β-LUMO occupy practically the same part of the space, involving approximately 1.098 and 0.902 electrons. The same situation is found in the case of the β-HOMO and α-LUMO. In this way, there are no unpaired electrons in even system, yet two of them occupy different parts of the space with a small shared region indicating that the ground state is singlet biradical and thus allowing the π-electrons to delocalize.

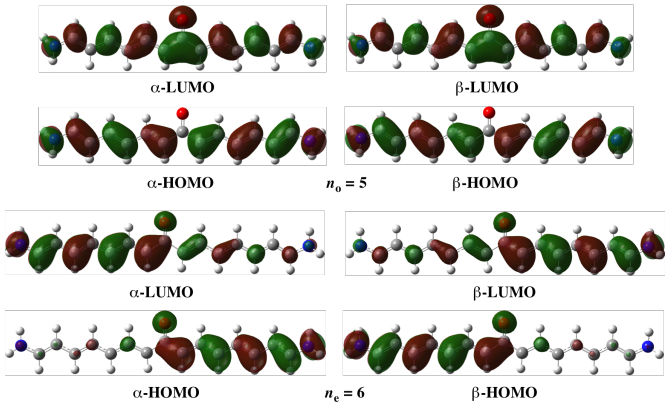

Fig. 4 Frontier one electron molecular orbitals of the KCYs for n_o = 5 (top) and n_e = 6 (bottom).

It is also important to inspect the spin densities of the singlet biradicals. The Mulliken spin density distribution at each carbon atom of the chain for n_e series is shown in Figure of Table 3 while the sum of spin densities on the left and right side of the *meso*-position and the spin densities at the C_3 and $C_{3'}$ carbon atoms are presented in Table **3**. The very small or negligible spin density alternation (spin up (↑) and spin down (↓)) along the π-conjugation in n_o series does not confirm the spin alternation and indeed indicate the absence of the biradical character. The sums of spin densities in n_e series increase with conjugation length due to the delocalization of spins over the π-conjugation and decrease at C_3 and $C_{3'}$ atoms. This indeed implies that the coupling between the unpaired electrons is reduced leading to large biradical character. For shorter chain lengths, the spins localize at C_3, $C_{3'}$ positions and start moving towards the centre of the aminopolyenic chromophores with increasing length. Moreover, the spin densities with opposite signs on either side of the *meso*-position indicate the localization of the spin up (↑) and spin down (↓) electrons and hence the stability of the singlet biradical in the ground state. Beyond the critical value for n_e, a simple inversion in the sign of spin density from negative to positive or vice-versa occurs which leads to the stability of the triplet state. Since the biradical character for n_e = 2 is ~50%, it is not possible to predict the spin densities.

Table 3 Singlet ground state spin densities of n_e series located at each carbon atom of the polymethine (figure) and at C_3 and $C_{3'}$ carbon atoms and summed spin densities located at left and right polymethine chains.

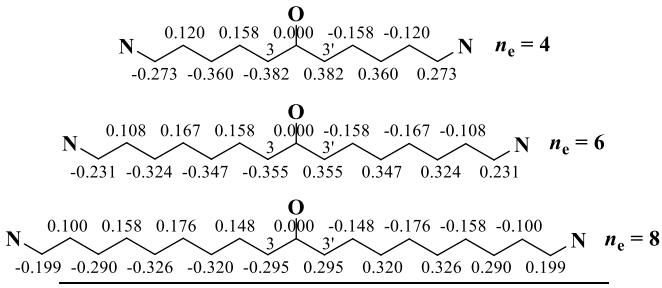

n_e	Left chain	C_3	$C_{3'}$	Right chain
4	0.829	0.382	-0.382	-0.783
6	0.881	0.335	-0.335	-0.833
8	0.704	0.295	-0.295	-0.863

3.4. Frontier Molecular Orbitals

A comparison of five highest occupied and five lowest unoccupied levels for both the series is shown in Fig. **5**. The sensitivity of the chain length dependence of n_o series can be seen from the continuous destabilization of the HOMO level from -5.6 to -4.8 eV and stabilization of LUMO level from -0.78 to -2.11 eV. This can be explained based on the atomic coefficients for the HOMO and LUMO orbitals as depicted in Fig. **6** (top). The HOMO in each of the n_o series is characterized by a nodal plane through O_1 and C_2 atoms, which primarily indicates that it lacks the KCY character (concentration of electron density at C_3–C_2–$C_{3'}$ atoms) in the S_0 state. One would expect a little contribution from these two atoms to the HOMO level. The coefficients at C_3, C_5, C_7, and C_9 (equivalent positions $C_{3'}$, $C_{5'}$, $C_{7'}$, and $C_{9'}$) are relatively large than those at C_4, C_6, C_8 and C_{10} ($C_{4'}$, $C_{6'}$, $C_{8'}$ and $C_{10'}$) atoms. Also, the coefficients decrease along the polymethine chain as n_o increases. Moreover, the coefficients at C_3 and $C_{3'}$ continuously decrease (0.57–0.34) and consequently the energy of the HOMO is raised. The LUMO is characterized by a large contribution from O_1 and C_2 atoms such that increasing the n_o is expected to affect the LUMO and the n_o series retains the KCY character. Interestingly, the coefficients at C_3, C_5, C_7, and C_9 (equivalent positions $C_{3'}$, $C_{5'}$, $C_{7'}$, and $C_{9'}$) are relatively smaller than those at C_4, C_6, C_8 and C_{10} ($C_{4'}$, $C_{6'}$, $C_{8'}$ and $C_{10'}$). The coefficients at C_3 and $C_{3'}$ are in phase with C_2 and therefore the increase of coefficient at C_3 and $C_{3'}$ continuously stabilize the LUMO with increasing n_o. At the same time the coefficient at C_3 and $C_{3'}$ in the HOMO are in out of phase relation with the C_2 therefore decrease of the coefficient at C_3 and $C_{3'}$ continuously destabilize the HOMO with increasing n_o. This consequently decreases the HLG with increasing n_o (Fig. **5**). This suggests that the decrease of HLG is driven by both HOMO and LUMO.

Contrary to n_o series, the HOMO in each of the n_e series is characterized by a large coefficient at O_1 and C_2 atoms indicating that the KCY character is maintained. Increasing n_e, the coefficient at O_1 is decreased (0.64–0.43) while a constant coefficient at C_2 (0.11) is maintained Fig. **6** (bottom). As seen in Fig. **5**, the constant position of HOMO level at -3.8 eV with n_e is attributed to the constant coefficient at C_2 atom. The coefficients at the rest of the carbon atoms along the chain have similar coefficients as in n_o series. The LUMO in this series is characterized by a nodal plane through O_1 and C_2 atoms and the coefficients at C_3, C_5, C_7, and C_9 (equivalent positions $C_{3'}$, $C_{5'}$, $C_{7'}$, and $C_{9'}$) are relatively larger than those in the HOMO while the coefficients at C_4, C_6, C_8 and C_{10} ($C_{4'}$, $C_{6'}$, $C_{8'}$ and $C_{10'}$) is negligible. The continuous stabilization of LUMO (from -2.22 to -3.0 eV) is attributed to the decrease in the coefficients at C_3 and $C_{3'}$. Thus the decrease of HLG in n_e series is LUMO driven.

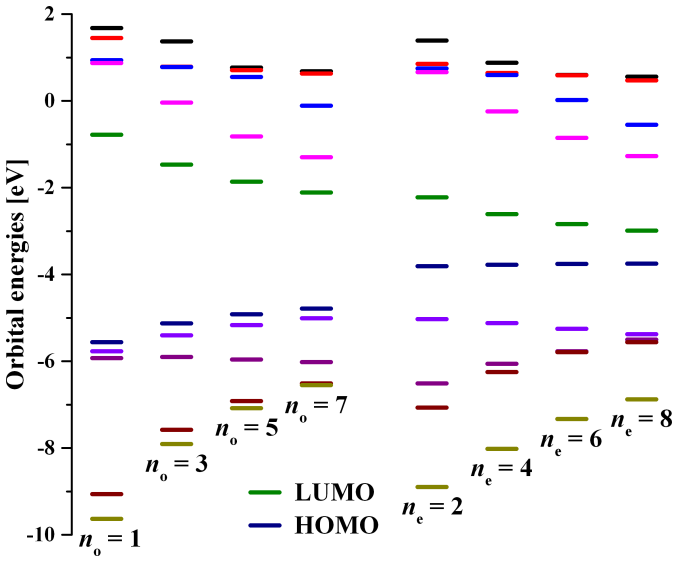

Fig. 5 Evolution of energy levels of five highest occupied and five lowest unoccupied levels of n_o and n_e series of KCYs.

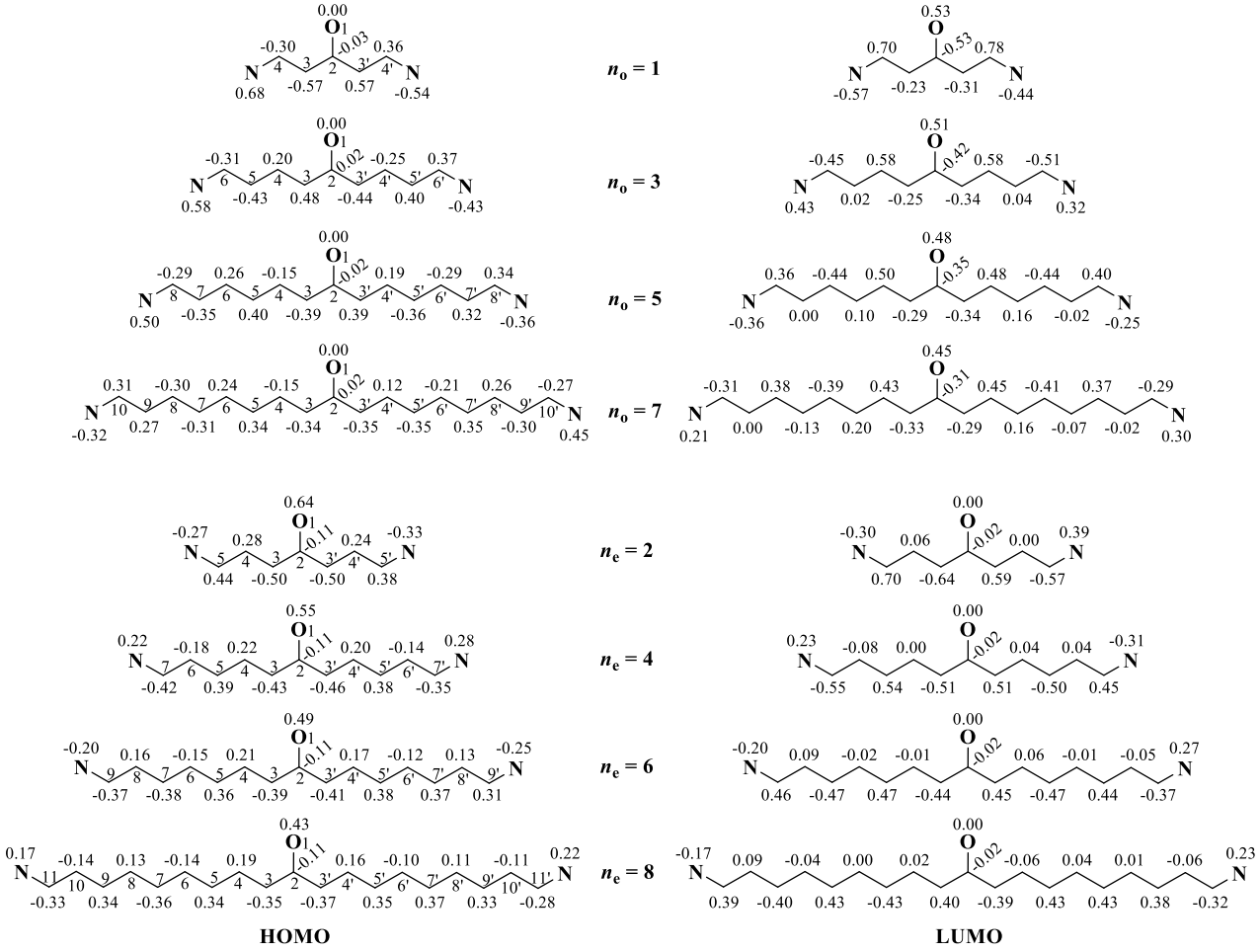

Fig. 6 HOMO and LUMO coefficients for odd (top) and even (bottom) KCY series.

3.5. Vertical Electronic Transition Energies

The photophysical properties of both the series of KCYs are qualitatively well described by the "free electron" model and represented by two potential boxes corresponding to the two aminopolyenic chromophore units separated by a potential barrier while the length of the chromophore corresponds to the width of the box, Fig. **7**. The barrier is due to the presence of C=O group. The difference between both the series lies in the strength of coupling between aminopolyene chromophores with CO group. The barrier is so high in the n_o series due to the very small coupling between the two aminopolyeneic chromophores (cross-conjugation) and it vanishes in the even series due to the strong coupling of the chromophores (increased conjugation). Depending upon the strength of the coupling between the aminopolyenic chromophores, the electronic coupling between the excited singlet states in both the series can occur in two ways as shown in the Fig. **7**. (i) dipole-dipole interaction and (ii) conjugation through the potential barrier and corresponds to the electron tunnelling through the barrier. The dipole-dipole interaction in odd systems is very weak due to the presence of cross-conjugation (aminopolyeneal and aminopolyene are treated as isolated dipoles). This interaction gives the small symmetric splitting (Δν, a measure of the chromophore interaction) between the S_1 and S_2 excited states leading to the symmetry allowed $S_0 \rightarrow S_1$ and symmetry forbidden $S_0 \rightarrow S_2$ transitions, but symmetry allowed for two-photon absorption. In the case of even systems, the dipole-dipole interactions between the aminopolyenic chromophores are very strong due to increased conjugation, which result in the large symmetric splitting of S_1 and S_2 states. In addition to the dipole-dipole interactions, the conjugation results in the stabilization of both the S_1 and S_2 sates so that the final splitting becomes unsymmetric (Fig. **7**). This will relatively decrease E_{01} and increase E_{02} by making $S_0 \rightarrow S_2$ transition symmetrically forbidden for both one- and two-photon absorption.

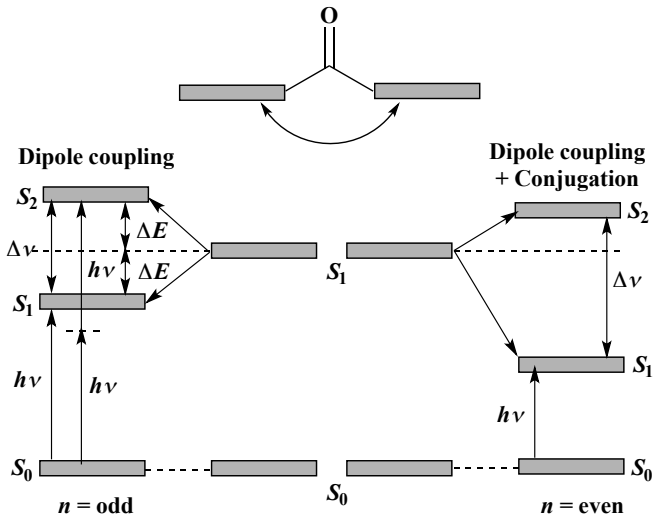

Fig. 7: Interaction of chromophores in their singlet excited states.

To quantify the above discussion, the calculated lowest optically allowed E_{01}, corresponding μ_{01}, μ_0 and μ_1 for both n_o and n_e series and their corresponding nature of transitions at the orbital level for singles ($C_i^{singles} \geq 0.1$) and doubles ($C_i^{doubles} \geq 0.2$) are collected in Table **4**. For n_o series, large E_{01} ($S_0 \rightarrow S_1/\pi \rightarrow \pi^*$), values of 4.95 ($n_o$ = 1), 3.99 (n_o = 3), 3.45 (n_o = 5) and 3.37 eV (n_o = 7) ($1^1A \rightarrow 1^1B$) are produced with a large intensity as evident from their respective μ_{01} values of 7.1, 10.1, 12.9 and 15.5 D and are polarized along *y*-direction. These values are in good agreement with the energy gap (HLG) of 4.77, 3.66, 3.06 and 2.68 eV as shown in Table **2**. The calculated trend is in good agreement with the experiment but the values differ by ~1.32 eV (experimentally determined values are 3.54, 2.64 and 2.25 eV for n_o = 1, 3 and 5 respectively).[75] This deviation is due to the fact that the measurements were performed in the solution phase while the calculations are performed in the gas phase. Though quantitatively the experimental values cannot be reproduced, the trends and the responsible factors can be reasoned. At the orbital level these transitions are described as a single particle-hole excitation from the HOMO→LUMO ($a \rightarrow b$) level with a single $|c_i|$ of 0.944, 0.935, 0.914 and 0.893 respectively as depicted in Fig. **4**. These transitions are also accompanied by a less prominent but with significant $|c_i|$ value of 0.125, 0.200, 0.268 and 0.323 along the series from low lying occupied to higher lying unoccupied orbitals HOMO-1→LUMO+3/HOMO-1→LUMO+1 ($b \rightarrow a/b \rightarrow a$). These large energy transitions in n_o series are in fact due to the presence of cross-conjugation (no interaction between aminopolyeneal and aminopolyene chromophores, structure **c** of Fig. **1**) which reduces the effective conjugation length. The decrease in the E_{01} energy with increase in n_o is due to the delocalization of the π-electron cloud across aminopolyenenal chromophore. At the same time, increasing the conjugation on the other aminopolyeneic chromophore has no impact on these transitions but simply extends the conjugation length. The very small increase from n_o = 5 to 7 suggests the saturation limit which is evident from the large BLA value of 0.08 Å (Fig. **3**). Beyond this optimal length of n_o = 7, the BLA would reach the maximum value of 0.1 Å, equivalent to that of typical polyene and thus would not show further decrease in E_{01}. The second lowest transition energies E_{02} ($S_0 \rightarrow S_2/\pi \rightarrow \pi^*$, two-photon state) appeared at 5.04, 4.41, 3.96 and 3.95 eV ($1^1A \rightarrow 3^1A/1^1A \rightarrow 4^1A$). These transitions are *z*-polarized and have relatively small intensity as seen from the μ_{02} values (Table **4**). These transitions are described as HOMO-1→LUMO ($b \rightarrow b$) and accompanied by HOMO→LUMO+1/HOMO-3→LUMO ($a \rightarrow a/b \rightarrow b$). The small splitting, Δν between S_1 and S_2 states of 730, 3390, 4110 and 4680 cm^{-1} (0.09, 0.42, 0.51 and 0.58 eV) for n_o = 1, 3, 5 and 7 suggest that the interaction between the aminopolyeneal and aminopolyene chromophores is very small and increase with n_o. This favors symmetrically allowed two-photon transition between the S_0 and S_2 states.

Table 4 Calculated $S_0 \rightarrow S_1$ and $S_0 \rightarrow S_2$ transition energies (E_{0i}, eV), S_0 and S_1 permanent dipole moments and $S_0 \rightarrow S_1$ transition dipole moments (μ_0, μ_1 and μ_{0i}, D), nature of the transitions ($C_i^{singles} \geq 0.1$ & $C_i^{doubles} \geq 0.2$) and splitting between S_1 and S_2 states (Δν, cm^{-1}). The directions of the dipole moments are given in parenthesis. [a,b] i = 1 for $S_0 \rightarrow S_1$ and 2 for $S_0 \rightarrow S_2$ respectively for both the series of KCYs.

n	$^aE_{0i}$	*State*	μ_0	μ_i	$^b\mu_{0i}$	Nature of Transition	Δν
n_o series							
1	4.95	$1^1A \rightarrow 1^1B$	3.0(*z*)	4.8(*z*)	7.1(*y*)	0.944 (H→L) -0.125 (H-1→L+3)	730
	5.04	$1^1A \rightarrow 3^1A$		2.9(*z*)	1.1(*z*)	0.917 (H-1→L)	
3	3.99	$1^1A \rightarrow 1^1B$	2.4(*z*)	4.0(*z*)	10.1(*y*)	0.935 (H→L) +0.200 (H-1→L+1)	3390
	4.41	$1^1A \rightarrow 3^1A$		2.5(*z*)	0.4(*z*)	-0.848 (H-1→L) -0.170 (H-3→L)	
5	3.45	$1^1A \rightarrow 1^1B$	2.1(*z*)	3.5(*z*)	12.9(*y*)	0.914(H→L) +0.268 (H-1→L+1)	4110
	3.96	$1^1A \rightarrow 4^1A$		3.3(*z*)	0.4(*z*)	0.918 (H-1→L) +0.141 (H→L+1)	
7	3.37	$1^1A \rightarrow 1^1B$	1.8(*z*)	3.0(*z*)	15.5(*y*)	0.893 (H→L) -0.323 (H-1→L+1)	4680
	3.95	$1^1A \rightarrow 3^1A$		2.9(*z*)	0.6(*z*)	0.902 (H-1→L) -0.222 (H→L+1)	
n_e series							
2	1.57	$1^1A \rightarrow 1^1B$	4.5(*z*)	2.4(*z*)	9.7(*y*)	0.899 (H→L) +0.234 (H-2→L) -0.234 (H→L+1; H→L)	11940
	3.05	$1^1A \rightarrow 2^1A$		1.9(*z*)	0.6(*z*)	0.603 (H→L+1) +0.361 (H-3→L) -0.503 (H→L; H→L)	
4	1.21	$1^1A \rightarrow 1^1B$	4.5(*z*)	3.1(*z*)	14.4(*y*)	0.902 (H→L) +0.174 (H-2→L) -0.240 (H→L+1; H→L)	19760
	2.45	$1^1A \rightarrow 2^1A$		2.3(*z*)	1.3(*z*)	-0.559 (H→L+1) -0.394 (H-1→L) -0.517 (H→L; H→L)	
6	1.21	$1^1A \rightarrow 1^1B$	4.4(*z*)	3.6(*z*)	19.1(*y*)	0.909 (H→L) +0.148 (H-4→L) -0.243 (H→L+1; H→L)	24360
	4.23	$1^1A \rightarrow 4^1A$		3.7(*z*)	0.5(*z*)	-0.381 (H→L+1) +0.282 (H-5→L) -0.641 (H→L; H→L)	
8	1.25	$1^1A \rightarrow 1^1B$	4.3(*z*)	3.9(*z*)	22.8(*y*)	0.902 (H→L) +0.143 (H-4→L) -0.272 (H→L+1; H→L)	25650
	4.43	$1^1A \rightarrow 4^1A$		3.0(*z*)	0.4(*z*)	-0.445 (H→L+1) -0.249 (H-5→L) +0.619 (H→L; H→L)	

The E_{01} energies of n_e series are relatively small compared to n_o series and showed absorption in the NIR region. The E_{01} ($S_0 \rightarrow S_1/\pi \rightarrow \pi^*$) values are 1.57 ($n_e$ = 2), 1.21 (n_e = 4), 1.21 (n_e = 6) and 1.25 (n_e = 8) eV ($1^1A \rightarrow 1^1B$) respectively. These values are also in good agreement with HLG (Table **2**). These transitions are appeared with large intensity as evident from their respective μ_{01} values of 9.7, 14.4, 19.1 and 22.8 D. These transitions are similar to n_o series but differ in the supplement transition. These are described as HOMO-2→LUMO/HOMO-4→LUMO ($b \rightarrow a/b \rightarrow a$) for the intermediate and large biradical systems. In addition to the singles CI, these are accompanied with doubles CI (common for biradicals) from HOMO→LUMO+1; HOMO→LUMO ($b \rightarrow b$; $b \rightarrow a$) with $|c_i|$ =0.234, 0.240, 0.243 and 0.272 respectively. As discussed earlier, the n_e series lose the oxyallyl characteristic (biradical nature and the concentration of electron density at the center) and increase in E_{01} values at n_e = 7. This is evident from the continuous increase in BLA up to 0.06 Å (Fig. **3**) and has been proved experimentally and theoretically for extended squaraines.[40] The second lowest transitions are *z*-polarized and the energies are 3.05, 2.45, 4.23 and 4.43 eV ($1^1A \rightarrow 2^1A/1^1A \rightarrow 4^1A$). These have relatively small intensity as seen from the μ_{02} values (Table **3**). These transitions are different from n_o series and described as HOMO→LUMO+1 ($b \rightarrow b$) and accompanied by single and doubles excitations HOMO-1→LUMO/ HOMO-3→LUMO/ HOMO-5→LUMO ($b \rightarrow b$), HOMO→LUMO; HOMO→LUMO ($b \rightarrow a$; $b \rightarrow a$). The very large splitting, Δν between the S_1 and S_2 states of 11940, 19760, 24360 and 25650 cm^{-1} (1.48, 2.45, 3.02 and 3.18 eV) for n_o = 2, 4, 6 and 8 suggest that the interaction between the aminopolyeneal and aminopolyene chromophores is very strong and increase with n_e. This makes the two-photon transition between the S_0 and S_2 states symmetrically forbidden.

The constant μ_0 values of 4.5 D for n_e indicate the presence of neutral biradical form in the S_0 state while the increase of μ_1 (both n_o and n_e series) in the S_1 state represent the charge-separated form. At sufficiently long chain length, both these systems might undergo symmetry-breaking in the excited state.[76] This is in contrast to the typical CY which show nearly equivalent μ_0 and μ_1 values up to a critical value of *n*, but under goes symmetry-breaking in the ground state at sufficiently long chain lengths.[51]

Based on these structure-property relations, it can be explained that the small energy absorption of 1.13 eV for BM1 dye reported by Langhals et. al[77] is due to the fact that it belongs to even series of KCYs and thus have a large biradical character. Extension by methine group on either side produces BM2 (furan to pyran),[78] which showed absorption energy of 2.76 eV and thus belongs to odd KCY series and thus possess small biradical character. Similarly, these relationships can applicable to explain the absorption of SQ and CR dyes reported by several authors.[18, 23, 29, 44, 79]

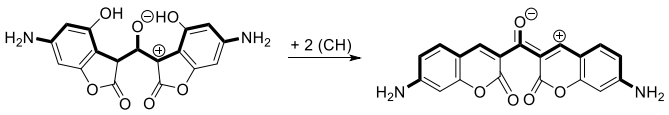

BM1 (n_e = 4) E_{01} = 1.13 eV **BM2 (n_o = 5)** E_{01} = 2.76 eV

Fig. 8 Example of KCY dyes with even and odd methane units.

3.6. Third-Order Polarizabilities:

The average static (at zero frequency) third-order polarizabilities, ⟨γ⟩ were calculated by fitting the quantities obtained from SACCI calculations into eq.(1) to eq.(3). The eq.(1) and eq.(2) assist to elucidate the major structural aspects that influence the origin of negative sign and the large magnitudes of KCYs. The T-term is calculated by considering the second excited state (two-photon state) that is strongly coupled to the first excited state with large transition dipole moments, μ_{12}. The calculated values for each of the D, N and T-terms (γ^D, γ^N and γ^T) and ⟨γ⟩ are presented in Table **5**. Irrespective of odd or even series, symmetric KCYs are characterized by non-vanishing dipole moments in S_0, S_1 and S_2 states along *z*-direction (C_2 symmetry) while the difference in dipole moment ($\Delta\mu_{01}^z$) remains only in the *z*-component. The molecular long axis is taken as *y* and *x* is perpendicular to the approximate plane of the molecule therefore the transition dipole moment between the two states, $S_0 \rightarrow S_1$ (μ_{01}) or $S_1 \rightarrow S_2$ (μ_{02}) is limited to *x* and *y*-directions. By using these symmetry relations, eq.(1) and eq.(2) are reduced to eq.(5) and eq.(6) as shown:

$$\gamma_{iiii} = 24\left[-\frac{(\mu_{01}^i)^4}{(E_{01})^3} + \frac{(\mu_{01}^i)^2(\mu_{12}^i)^2}{(E_{01})^2 E_{02}}\right] = \gamma_{iiii}^N + \gamma_{iiii}^T;\ iiii \in \{xxxx, yyyy\} \quad \text{eq.(5)}$$

$$\gamma_{iijj} = 4\left[\frac{(\mu_{01}^i \Delta\mu_{01}^j)^2}{(E_{01})^3}\right] = \gamma_{iijj}^D; iijj \in \{xxzz, yyzz\}$$

$$\gamma_{iijj} = 4\left[-\frac{6(\mu_{01}^x\mu_{01}^y)^2}{(E_{01})^3} + \frac{4\mu_{01}^x\mu_{12}^x\mu_{01}^y\mu_{12}^y + (\mu_{01}^x\Delta\mu_{12}^y)^2 + (\mu_{01}^y\Delta\mu_{12}^x)^2}{(E_{01})^2 E_{02}}\right] = \gamma_{xxyy}^N + \gamma_{xxyy}^T \quad \text{eq.(6)}$$

Under the three-state approximation, the *z*-component γ_{zzzz} is vanished. From the table it is seen that both the series possess negative ⟨γ⟩ values mainly originate from the $S_0 \rightarrow S_1$ transition dipole moments (7.1–15.5 D, 9.7–22.8 D for both the series) indicating the predominance of γ^N term. Moreover, the values of n_e series is 2–4 orders of magnitude larger than the n_o series. The factors to these contributions can be depicted in detail as follows. (i) The small S_0 and S_1 state dipole moment difference ($\Delta\mu_{01}^z$) (0.4–2.1 D) which produce non-compensating and insignificant contribution of < 2.0 % (0.5 – 3.3×10^{-36} esu and 39.6 – 14.9×10^{-36} esu) from the D-term (γ_{xxzz}^D and γ_{yyzz}^D) in both the series. These small values are originated by the amino groups, which are projected in the *x*-direction (as the hydrogen atoms of amino group is projected in *x*-direction). (ii) A very large significant reduction of the ⟨γ⟩ values in n_o series by 43-98 % is mainly due to compensatory contributions from the γ^T term (10.4–1702.5×10^{-36} esu) originating from $S_1 \rightarrow S_2$ ($1^1B \rightarrow 2^1A$) transition dipole moments, μ_{12} of 4.7–16.6 D (two-photon transition probability). Moreover, $S_0 \rightarrow S_2$ transition, which is one-photon forbidden in centro-symmetric systems, becomes two-photon allowed with *y* polarization due to small $S_1 \rightarrow S_2$ energy gap (0.09-0.58 eV) (Table **4**). (iii) In the case of even series, the large values originate from very large $S_0 \rightarrow S_1$ transition dipole moments (9.7–22.8 D) and introduces ~12.0 % (252.8–2811.9×10^{-36} esu) compensating contribution originating from the small μ_{12} (4.0-5.5 D) due to large $S_1 \rightarrow S_2$ energy gap (1.24–3.18 eV), making ⟨γ⟩ to be very large in negative (as in ideal CYs). Thus, very large μ_{12} transition dipole moment represents a crucial factor that discriminates the n_o and n_e series of KCYs. However, for both γ^D and γ^N, the *y*-component (γ_{yyyy} and γ_{yyzz}) dominates over *x* (<1.5 %) due to the large transition moments in *y*-direction (along the carbon chain). In contrast, the symmetric CYs have a strong contribution from $S_0 \rightarrow S_1$ transition giving rise to large negative ⟨γ⟩ while for the asymmetric CYs (beyond the critical chain length where the onset of symmetry-breaking occurs), ⟨γ⟩ is large and positive due to the compensating contribution from the D- and T-terms.[53] The contribution from the higher excited states is negligible, as the transitions from ground to higher excited states ($S_0 \rightarrow S_i$; i ≥ 2) and from first excited state to the higher two-photon states ($S_1 \rightarrow S_j$; j ≥ 3) are associated with large E_{0i},

E_{1j} and weak μ_{0i} and μ_{1j}, the net contribution to N and T-terms become negligible. This can be demonstrated by considering the shortest KCY in n_e series (n_e = 2). Further, taking into account that $S_0 \rightarrow S_1$ is the dominant contributor while contributions from $S_0 \rightarrow S_i$ (i ≥ 2) are negligible it is important to consider the effect from the higher two-photon transitions ($S_1 \rightarrow S_j$; j ≥ 3). In light of these approximations, the contribution from $S_1 \rightarrow S_3$ and $S_1 \rightarrow S_4$ are 62.3×10^{-36} (2.5%) and 3.4×10^{-36} esu (0.13 %) leading to a $\langle\gamma\rangle$ of 2528.5×10^{-36} and 2587.3×10^{-36} esu. These values are very close to the $\langle\gamma\rangle$ values, -2590.7×10^{-36} and -2337.9×10^{-36} esu obtained under two-state and three-state approximation. This clearly demonstrates the convergence in the $\langle\gamma\rangle$ values and at the same time insignificance of the higher two-photon states. Further, the values of $\langle\gamma\rangle^{2\text{-state}}$ and $\langle\gamma\rangle^{3\text{-state}}$, indicate that the three-states approximation has a strong impact on the $\langle\gamma\rangle$ values. For the n_o series, the $\langle\gamma\rangle$ values appeared to be converged with the three-state approximation while for n_e series it appeared to be satisfactorily converged with the two-state approximation. In addition, the large $\langle\gamma\rangle$ values of n_e series is attributed to the large biradical character which is in line with the earlier predictions.[43] We conclude that it is important to account at least three states to explain and design new materials for large negative $\langle\gamma\rangle$ derived from KCY.

Using these structure-property relationships, the large negative $\langle\gamma\rangle$ in BM1 and BM2 can be simply explained as they belong to even and odd KCY series. Similarly, these relationships can applicable to explain the large negative third-order polarizabilities of SQ and CR dyes reported by several authors.[24, 44, 80]

Table 5 Calculated $S_0 \rightarrow S_1$ and $S_1 \rightarrow S_2$ transition dipole moments, contributions of dipolar, negative and two-photon terms (γ^D, γ^N and γ^T, $\times10^{-36}$ esu) and average $\langle\gamma\rangle$ at 2-state and 3-state model ($\langle\gamma\rangle^{2\text{-state}}$and $\langle\gamma\rangle^{3\text{-state}}$, $\times10^{-36}$ esu) for both the series of KCYs.

n	μ_{01}	μ_{12}	γ^D	γ^N	γ^T	$(\langle\gamma\rangle^{2\text{-state}}$	$\langle\gamma\rangle^{3\text{-state}}$
n_o series							
1	7.1	4.7	0.5	-24.2	10.4	-23.7	-13.3
3	10.1	5.2	1.7	-191.4	45.7	-189.7	-144.0
5	12.9	14.6	3.1	-795.1	675.8	-792.0	-84.3
7	15.5	16.6	3.3	-1738.4	1702.5	-1735.1	-32.5
n_e series							
2	9.7	4.2	39.6	-2630.3	252.8	-2590.7	-2337.9
4	14.4	6.5	92.8	-27931.1	2811.9	-27838.3	-25026.3
6	19.1	4.0	59.2	-87406.0	1101.4	-87346.8	-86245.4
8	22.8	5.5	14.9	-163069.9	2631.8	-163055.0	-160423.0

4. Conclusions

We have performed detailed calculations to understand the electronic structure, optical absorption and third-order polarizabilities of symmetric KCYs containing odd and even number of methine units in the carbon backbone. The results address the following predictions. (i) The very small interaction between the aminopolyeneal and aminopolyene chromophores in odd series of KCYs suggests that these are cross-conjugated systems and the instability of the closed shell ground state wavefunction of even series suggests that they exist in the form of biradicals. (ii) The presence of cross-conjugation reduces the effective conjugation length which is reflected in the large $S_0 \rightarrow S_1$ transition energies (blue region of the spectrum). The biradicaloid character or the mixture of biradical and charge-separated forms increases the overlap between the two chromophores and consequently reduces the HLG. This is clearly reflected in the small and intense $S_0 \rightarrow S_1$ transition energies (NIR region). (iii) Overall this leads to a large negative values for $\langle\gamma\rangle$. The relatively small $\langle\gamma\rangle$ values in the odd series is predicted to be the compensating contribution from the T-term and originated from the large $S_1 \rightarrow S_2$ transition dipole moments due to small energy splitting between S_1 and S_2 states. The large negative values in the even series is originated from the large $S_0 \rightarrow S_1$ transition moments and very small compensating contribution from the $S_1 \rightarrow S_2$ transition moments due to the large splitting between the S_1 and S_2 states. (iv) The results also suggests that odd series requires at least three-states, while even series requires two-states to model the KCYs and to determine the values of $\langle\gamma\rangle$. Thus, in short, excluding the core oxyallyl part, KCYs containing odd number of methine units absorbs in visible region and show small negative $\langle\gamma\rangle$ while KCYs with even number of methine units absorb in the NIR region and show large negative $\langle\gamma\rangle$. Depending up on the type of application, this can be used as design principles for KCY systems for tuning the optical absorption from the visible to NIR region and subsequently leading to large third-order polarizabilities.

Acknowledgement

EDJ and KY thank Department of Science and Technology (DST), New Delhi for the support under J. C. Bose Fellowship. We also thank Center for Molecular Simulation and Design (CMSD), University of Hyderabad for computational facilities.

Notes and references

[a]*School of Chemistry, Indian Institute of Science Education and Research Thiruvananthapuram – 695 016, India.*

[b]*Currently at Department of Engineering Chemistry, GITAM University, Bangalore - 561 203, India.*

[c]*Currently at Inorganic and Physical Chemistry, Indian Institute of Science, Bangalore - 560 012, India.*

[d]*Inorganic and Physical Chemistry Division, CSIR-Indian Institute of Chemical Technology, Uppal Road, Tarnaka, Hyderabad - 500 007, India.*

Corresponding Author Email: yesudas.kada@gmail.com

References

1. F. M. Hamer, *The cyanine dyes and related compounds*, Interscience Publishers, New York,, 1964.

2. A. Mishra, R. K. Behera, P. K. Behera, B. K. Mishra and G. B. Behera, *Chem. Rev.*, 2000, **100**, 1973-2012.
3. J. L. Bredas, C. Adant, P. Tackx, A. Persoons and B. M. Pierce, *Chem. Rev.*, 1994, **94**, 243-278.
4. L. A. Padilha, S. Webster, O. V. Przhonska, H. Hu, D. Peceli, J. L. Rosch, M. V. Bondar, A. O. Gerasov, Y. P. Kovtun, M. P. Shandura, A. D. Kachkovski, D. J. Hagan and E. W. V. Stryland, *J. Mater. Chem.*, 2009, **19**, 7503-7513.
5. J. Wang, W.-F. Cao, J.-H. Su, H. Tian, Y.-H. Huang and Z.-R. Sun, *Dyes Pigm.*, 2003, **57**, 171-179.
6. M. Emmelius, G. Pawlowski and H. W. Vollmann, *Angew. Chem., Int. Ed.*, 1989, **28**, 1445-1471.
7. H. Tian and F. Meng, in *Functional Dyes*, ed. S.-H. Kim, Elsevier Science, Amsterdam2006, pp. 47-84.
8. X. J. Feng, P. L. Wu, F. Bolze, H. W. C. Leung, K. F. Li, N. K. Mak, D. W. J. Kwong, J.-F. Nicoud, K. W. Cheah and M. S. Wong, *Org. Lett.*, 2010, **12**, 2194-2197.
9. T. Deligeorgiev and A. Vasilev, in *Functional Dyes*, ed. S.-H. Kim, Elsevier Science, Amsterdam2006, pp. 137-183.
10. N. S. James, Y. Chen, P. Joshi, T. Y. Ohulchanskyy, M. Ethirajan, M. Henary, L. Strekowsk and R. K. Pandey, *Theranostics*, 2013, **3**, 692-702.
11. J. M. Lanzafame, A. A. Muenter and D. V. Brumbaugh, *Chem. Phys.*, 1996, **210**, 79-89.
12. J. M. Lanzafame, L. Min, R. J. D. Miller, A. Muenter and B. Parkinson, *Mol. Cryst. Liq. Cryst.*, 1991, **194**, 287-292.
13. J. O. Tocho, R. Duchowicz, L. Scaffardi, G. M. Blimes, R. Dipaolo and M. Murphy, *Trends Phys. Chem.*, 1992, **3**, 31-47.
14. F. Würthner, R. Wortmann, R. Matschiner, K. Lukaszuk, K. Meerholz, Y. DeNardin, R. Bittner, C. Bräuchle and R. Sens, *Angew. Chem., Int. Ed.*, 1997, **36**, 2765-2768.
15. K. Sayama, K. Hara, Y. Ohga, A. Shinpou, S. Suga and H. Arakawa, *New J. Chem.*, 2001, **25**, 200-202.
16. Y. J. Ren, F. S. Meng, H. Tian and S. M. Cai, *Chin. Chem. Lett.*, 2002, **13**, 379-380.
17. R. Pandey, N. James, Y. Chen and M. Dobhal, in *Heterocyclic Polymethine Dyes*, ed. L. Strekowski, Springer Berlin Heidelberg2008, vol. 14, ch. 113, pp. 41-74.
18. T. P. Simard, J. H. Yu, J. M. Zebrowski-Young, N. F. Haley and M. R. Detty, *J. Org. Chem.*, 2000, **65**, 2236-2238.
19. H. Meier and U. Dullweber, *J. Org. Chem.*, 1997, **62**, 4821-4826.
20. C. Encinas, E. Otazo, L. Rivera, S. Miltsov and J. Alonso, *Tetrahedron Lett.*, 2002, **43**, 8391-8393.
21. L. Beverina, R. Ruffo, G. Patriarca, F. D. Angelis, D. Roberto, S. Righetto, R. Ugo and G. A. Pagani, *J. Mater. Chem.*, 2009, **19**, 8190-8197.
22. E. Collini, S. Carlotto, C. Ferrante, R. Bozio, A. Polimeno, J. Bloino, V. Barone, E. Ronchi, L. Beverina and G. A. Pagani, *Phys. Chem. Chem. Phys.*, 2011, **13**, 12087-12094.
23. M. Bala Murali Krishna and D. Narayana Rao, *J. Appl. Phys.*, 2013, **114**, 133103-133108.
24. Z. Li, Z.-h. Jin, K. Kasatani, H. Okamoto and S. Takenaka, *Japanese Journal of Applied Physics*, 2005, **44**, 4956.
25. Z. Li, Z.-h. Jin, K. Kasatani and H. Okamoto, *Physica B: Condensed Matter*, 2006, **382**, 229-234.
26. Y. Chen, Y. Zhu, D. Yang, Q. Luo, L. Yang, Y. Huang, S. Zhao and Z. Lu, *Chem. Commun.*, 2015, **51**, 6133-6136.
27. D. Yang, Q. Yang, L. Yang, Q. Luo, Y. Huang, Z. Lu and S. Zhao, *Chem. Commun.*, 2013, **49**, 10465-10467.
28. U. Mayerhoffer, K. Deing, K. Gruss, H. Braunschweig, K. Meerholz and F. Wurthner, *Angew. Chem., Int. Ed.*, 2009, **48**, 8776-8779.
29. B. Ananda Rao, K. Yesudas, G. Siva Kumar, K. Bhanuprakash, V. Jayathirtha Rao, G. D. Sharma and S. P. Singh, *Photochem. Photobiol. Sci.*, 2013, **12**, 1688-1699.
30. H. Choi, P. K. Santra and P. V. Kamat, *ACS Nano*, 2012, **6**, 5718-5726.
31. S. F. Volker, A. Schmiedel, M. Holzapfel, C. Bohm and C. Lambert, *Phys. Chem. Chem. Phys.*, 2013, **15**, 19831-19844.
32. B. Oswald, L. Patsenker, J. Duschl, H. Szmacinski, O. S. Wolfbeis and E. Terpetschnig, *Bioconjugate Chemistry*, 1999, **10**, 925-931.
33. E. Terpetschnig, H. Szmacinski, A. Ozinskas and J. R. Lakowicz, *Analytical Biochemistry*, 1994, **217**, 197-204.
34. K. Y. Law, *Chem. Rev.*, 1993, **93**, 449-486.
35. J. Fabian, H. Nakazumi and M. Matsuoka, *Chem. Rev.*, 1992, **92**, 1197-1226.
36. K. Y. Law and F. C. Bailey, *J. Org. Chem.*, 1992, **57**, 3278-3286.
37. C. W. Dirk, L.-T. Cheng and M. G. Kuzyk, *Int. J. Quantum Chem.*, 1992, **43**, 27-36.
38. R. W. Bigelow and H.-J. Freund, *Chem. Phys.*, 1986, **107**, 159-174.
39. F. Momicchioli, A. S. Tatikolov, D. Vanossi and G. Ponterini, *Photochem. Photobiol. Sci.*, 2004, **3**, 396-402.
40. C. Prabhakar, K. Yesudas, G. K. Chaitanya, S. Sitha, K. Bhanuprakash and V. J. Rao, *J. Phys. Chem. A*, 2005, **109**, 8604-8616.
41. K. Srinivas, C. Prabhakar, C. L. Devi, K. Yesudas, K. Bhanuprakash and V. J. Rao, *J. Phys. Chem. A*, 2007, **111**, 3378-3386.
42. A. L. Puyad, C. Prabhakar, K. Yesudas, K. Bhanuprakash and V. Jayathirtha Rao, *J. Mol. Struct.: THEOCHEM*, 2009, **904**, 1-6.
43. K. Yesudas and K. Bhanuprakash, *J. Phys. Chem. A*, 2007, **111**, 1943-1952.
44. C. Prabhakar, K. Yesudas, K. Bhanuprakash, V. J. Rao, R. S. Santosh Kumar and D. N. Rao, *J. Phys. Chem. C*, 2008, **112**, 13272-13280.
45. J. Fabian and R. Peichert, *J. Phys. Org. Chem.*, 2010, **23**, 1137-1145.
46. P. Hohenberg and W. Kohn, *Phys. Rev.*, 1964, **136**, B864-B871.
47. W. Kohn and L. J. Sham, *Phys. Rev.*, 1965, **140**, A1133-A1138.
48. R. G. Parr and W. Yang, *Density Functional Theory of Atoms and Molecules*, Clarendon Press; Oxford University Press, Oxford, New York, 1989.
49. E. Gross, J. Dobson and M. Petersilka, in *Density Functional Theory II*, ed. R. Nalewajski, Springer Berlin / Heidelberg1996, vol. 181, pp. 81-172.
50. R. Bauernschmitt and R. Ahlrichs, *Chem. Phys. Lett.*, 1996, **256**, 454-464.
51. J. Fabian, *J. Mol. Struct.: THEOCHEM*, 2006, **766**, 49-60.
52. T. D. Iordanov, J. L. Davis, A. E. Masunov, A. Levenson, O. V. Przhonska and A. D. Kachkovski, *Int. J. Quantum Chem.*, 2009, **109**, 3592-3601.
53. K. Yesudas, *Phys. Chem. Chem. Phys.*, 2013, **15**, 19465-19477.
54. M. J. Frisch, G. W. Trucks, H. B. Schlegel, G. E. Scuseria, M. A. Robb, J. R. Cheeseman, J. A. Montgomery Jr., T. Vreven, K. N. Kudin, J. C. Burant, J. M. Millam, S. S. Iyengar, J. Tomasi, V. Barone, B. Mennucci, M. Cossi, G. Scalmani, N. Rega, G. A. Petersson, H. Nakatsuji, M. Hada, M. Ehara, K. Toyota, R. Fukuda, J. Hasegawa, M. Ishida, T. Nakajima, Y. Honda, O. Kitao, H. Nakai, M. Klene, X. Li, J. E. Knox, H. P. Hratchian, J. B. Cross, V. Bakken, C. Adamo, J. Jaramillo, R. Gomperts, R. E. Stratmann, O. Yazyev, A. J. Austin, R. Cammi, C. Pomelli, J. W. Ochterski, P. Y. Ayala, K. Morokuma, G. A. Voth, P. Salvador, J. J. Dannenberg, V. G. Zakrzewski, S. Dapprich, A. D. Daniels, M. C. Strain, O. Farkas, D. K. Malick, A. D. Rabuck, K. Raghavachari, J. B. Foresman, J. V. Ortiz, Q. Cui, A. G. Baboul, S. Clifford, J. Cioslowski, B. B. Stefanov, G. Liu, A. Liashenko, P. Piskorz, I. Komaromi, R. L. Martin, D. J. Fox, T. Keith, M. A. Al-Laham, C. Y. Peng, A. Nanayakkara, M. Challacombe, P. M. W. Gill, B. Johnson, W. Chen, M. W. Wong, C. Gonzalez and J. A. Pople, Gaussian Inc., Wallingford CT, A.02 edn., 2009.
55. A. D. Becke, *J. Chem. Phys.*, 1993, **98**, 5648-5652.
56. T. Nakajima and H. Nakatsuji, *Chem. Phys.*, 1999, **242**, 177-193.
57. T. Nakajima and H. Nakatsuji, *Chem. Phys. Lett.*, 1999, **300**, 1-8.
58. K. Toyota, M. Ishida, M. Ehara, M. J. Frisch and H. Nakatsuji, *Chem. Phys. Lett.*, 2003, **367**, 730-736.
59. B. J. Orr and J. F. Ward, *Mol. Phys.*, 1971, **20**, 513-526.
60. R. Bauernschmitt and R. Ahlrichs, *J. Chem. Phys.*, 1996, **104**, 9047-9052.
61. A. Thomas, K. Srinivas, C. Prabhakar, K. Bhanuprakash and V. J. Rao, *Chem. Phys. Lett.*, 2008, **454**, 36-41.
62. P.-O. Löwdin, *Phys. Rev.*, 1955, **97**, 1509-1520.
63. P. Lykos and G. W. Pratt, *Rev. Mod. Phys.*, 1963, **35**, 496-501.

64. K. Yamaguchi, T. Kawakami, Y. Takano, Y. Kitagawa, Y. Yamashita and H. Fujita, *Int. J. Quantum Chem.*, 2002, **90**, 370-385.
65. W. J. Hehre, *Ab initio molecular orbital theory*, Wiley, New York, 1986.
66. A. Szabo and N. S. Ostlund, *Modern quantum chemistry : introduction to advanced electronic structure theory*, Dover Publications, Mineola, N.Y., 1996.
67. P.-O. Löwdin, *Rev. Mod. Phys.*, 1964, **36**, 966-976.
68. K. Yamaguchi, Y. Takahara, T. Fueno and K. N. Houk, *Theor. Chim. Acta*, 1988, **73**, 337-364.
69. K. Yamaguchi, M. Okumura, W. Mori, J. Maki, K. Takada, T. Noro and K. Tanaka, *Chem. Phys. Lett.*, 1993, **210**, 201-210.
70. S. Dähne and R. Radeglia, *Tetrahedron*, 1971, **27**, 3673-3693.
71. J. S. Craw, J. R. Reimers, G. B. Bacskay, A. T. Wong and N. S. Hush, *Chem. Phys.*, 1992, **167**, 77-99.
72. J. S. Craw, J. R. Reimers, G. B. Bacskay, A. T. Wong and N. S. Hush, *Chem. Phys.*, 1992, **167**, 101-109.
73. V. Bachler, G. Olbrich, F. Neese and K. Wieghardt, *Inorg. Chem.*, 2002, **41**, 4179-4193.
74. M. Nakano, T. Nitta, K. Yamaguchi, B. Champagne and E. Botek, *J. Phys. Chem. A*, 2004, **108**, 4105-4111.
75. A. S. Tatikolov, Z. A. Krasnaya, L. A. Shvedova and V. A. Kuzmin, *Int. J. Photoenergy*, 2000, **2**, 23-30.
76. F. Terenziani, A. Painelli, C. Katan, M. Charlot and M. Blanchard-Desce, *J. Am. Chem. Soc.*, 2006, **128**, 15742-15755.
77. H. Langhals, *Angew. Chem., Int. Ed.*, 2003, **42**, 4286-4288.
78. D. P. Specht, P. A. Martic and S. Farid, *Tetrahedron*, 1982, **38**, 1203-1211.
79. H. Meier, R. Petermann and J. Gerold, *Chem. Commun.*, 1999, 977-978.
80. S. Tatsuura, M. Tian, M. Furuki, Y. Sato, I. Iwasa and H. Mitsu, *Appl. Phys. Lett.*, 2004, **84**, 1450-1452.

